INTERNATIONAL JOURNAL OF HYDROGEN ENERGY XXX (2011) 1–9

Available at www.sciencedirect.com

journal homepage: www.elsevier.com/locate/he

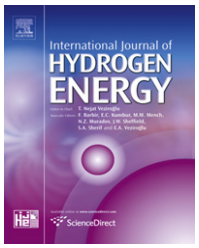

Role of initial conditions in unstably stratified hydrogen-air mixing zones

*Aaron A. Haley, Arindam Banerjee**

Department of Mechanical & Aerospace Engineering, Missouri University of Science and Technology (formerly University of Missouri-Rolla), Rolla, Missouri 65409, USA

ARTICLE INFO

Article history:
Received 25 January 2011
Received in revised form
29 May 2011
Accepted 1 June 2011
Available online xxx

Keywords:
Transient hydrogen mixing
Initial conditions

ABSTRACT

Characterization of the transient development of flammability zones from hydrogen leakage is often investigated through computational fluid dynamics simulation in order to predict the onset of hazardous ignition conditions. Without explicit consideration given to the effect of the initial conditions however, the generality of these efforts to predict the time-dependent mixing may suffer. In the present work, simulations of unstably-stratified hydrogen and air with various initial conditions allow the quantification of sensitivity of hydrogen dispersion to initial conditions. Development of turbulent mixing between a binary hydrogen-air system and propagation of flammability zones is studied using third-order accurate implicit large-eddy simulation. We find large wavelengths in the initial conditions contribute to faster propagation of the fuel first-arrival boundary and lower flammability envelope—important when considering accidental ignition. The results provide data necessary for predictive mix models of flammability zones propagation within enclosures.

Copyright © 2011, Hydrogen Energy Publications, LLC. Published by Elsevier Ltd. All rights reserved.

1. Introduction

Driven by the increasing need for clean-burning portable energy, hydrogen fuels and related technology offer an attractive alternative to hydrocarbon-based fuels. Lower emissions, the ability to be generated from renewable sources [1], and relative abundance are primary reasons that hydrogen fuels are favored as a clean source of energy for the transportation sector [2]. A prerequisite to the large scale use of hydrogen is that risks associated with its usage must be well understood, quantified, and aptly offset by appropriate safety codes and technologies. Being a colorless, odorless gas, hydrogen poses a unique risk as it mixes readily with air, and has a lower ignition energy than other fuels. An accidental release of hydrogen can quickly result in fire and explosion hazards without the user being made immediately aware. With a density 14.4 times lighter than air, buoyancy causes hydrogen leaks or spills to rapidly mix with ambient air creating a potentially large flammable volume [3]. Since the mixture formed is flammable over a large range of concentration (5%–75% hydrogen by volume), such risks are greatly enhanced over other common, but less buoyant, fuels such as methane or propane. Understanding the physics of hydrogen mixing in air is thus critical to a more complete understanding of the formation and behavior of flammable regions formed from accidental leakage, and is an essential part of the development of safety protocols and sensor technology to mitigate these risks.

Hydrogen leakage has been studied theoretically [4], experimentally [5–7], and using computational fluid dynamics (CFD) [3,8–12]. The advantages of this latter approach include control over the numerical experiment allowing precise

* *Corresponding author.*
E-mail address: banerjeea@mst.edu (A. Banerjee).

0360-3199/$ – see front matter Copyright © 2011, Hydrogen Energy Publications, LLC. Published by Elsevier Ltd. All rights reserved.
doi:10.1016/j.ijhydene.2011.06.001

Please cite this article in press as: Haley AA, Banerjee A, Role of initial conditions in unstably stratified hydrogen-air mixing zones, International Journal of Hydrogen Energy (2011), doi:10.1016/j.ijhydene.2011.06.001

specification of initial and boundary conditions, enhanced repeatability and lower risk than performing experiments with hydrogen. However, it also poses the risk of simulating leakage scenarios which are non-physical or cases where the initial conditions (ICs) are not explicitly characterized. Cisse & Karim [8] used a laminar 2D axis-symmetric Boussinesq model to investigate the transient mixing of a fixed mass of hydrogen and other gaseous fuels initially situated below a volume of air in standard atmosphere. The time of first arrival of the fuel at different axial locations showed that fuels with smaller molar mass mix faster than fuels with a heavier composition. The recent work of Fardisi & Karim [9] expand their earlier results [8] to 3D transient simulations in cylindrical geometries and note that 2D simulations tend to under predict mixing. Vudumu and Koylu [10] simulated hydrogen dispersion in a vertical enclosure modeled as a laminar 2D axis-symmetric flow with closed, open, or partially open top vertical boundary conditions. They find that for open configurations, growth of the hydrogen plume is hindered by an unfavorable pressure gradient with the closed top giving the shortest time for the hydrogen plume to reach the vertical domain boundary.

Hydrogen mixing in a vertical enclosure where a mass of hydrogen is initially situated below air follows the classical Rayleigh-Taylor (RT) instability. RT instability occurs when a higher-density fluid is placed above a lower density fluid in a gravitational field [13,14]. More specifically, instability exists if the pressure gradient opposes the density gradient (ie. $\nabla P \cdot \nabla \rho < 0$). In RT unstable flows, ICs are known to greatly affect dispersion and mixing [15,16]. Recent simulations investigating small-scale hydrogen leakages use an initially flat interface to initialize the problem domain [8–10]. A potential problem with this approach is that the small perturbations that are shown must develop from non-physical numerical effects. From linear stability theory [17] small single-mode interfacial perturbations in the linear regime (early time) grow exponentially according to:

$$h = h_0 \cosh(\Gamma t). \tag{1}$$

Ignoring viscous, interfacial, and other inhibiting effects, the growth rate, $\Gamma = \sqrt{A_t g/\lambda}$ is a function of the characteristic density ratio, $A_t = (\rho_1 - \rho_2)/(\rho_1 + \rho_2)$, gravity, g, and the perturbation wavelength, λ. Here the Atwood number, A_t is constrained to [0,1) so that ρ_1 and ρ_2 represent the density of the heavy and light fluids respectively. An initially flat interface is the limiting case where the perturbation height, $h_0 \to 0$ and $\lambda \to \infty$. In this case both the growth rate and initial interface height is zero for all time. This results in a quasi-stable solution where the problem degenerates to 1D diffusion. Since the ICs are not explicitly specified in earlier simulations [8–10], it is expected that code-specific numerical effects contribute to the development of initial interfacial perturbations. To reduce dependence on algorithmic details and make the result more general, it is important to characterize the initial interface by seeding appropriate perturbations into the flow [15].

In the present study, effect of ICs on hydrogen dispersion in air is examined through use of the 3D implicit large eddy simulation (ILES) code RTI-3D [18]. In addition, the necessity of explicit modeling of molecular diffusion in hydrogen mixing is investigated. Finally we analyze variable-density effects and argue the necessity to use non-Boussinesq governing equations when studying transient hydrogen dispersion in air. The rest of the paper is arranged as follows: §2 details of numerical simulation and methods; §3 covers setup of the problem; §4 discusses results from our simulations and offers design guidelines which may be used for safety codes. Finally in §5, we give our conclusions and recommendations.

2. Numerics

A third-order accurate ILES code [18] is used to solve the incompressible 3-D Euler equations. In the incompressible limit, the non-Boussinesq governing equations can be written as:

Continuity:

$$\frac{\partial u_j}{\partial x_j} = 0, \tag{2}$$

Species Transport:

$$\frac{D(\rho f_k)}{Dt} = \frac{\partial}{\partial x_j}\left(\mathcal{D}\rho \frac{\partial f_k}{\partial x_j}\right), \tag{3}$$

Momentum:

$$\frac{D(\rho u_i)}{Dt} = -\frac{\partial p}{\partial x_i} + \rho g_i, \tag{4}$$

where D/Dt represents the total (or material) derivative, ρ is the macroscopic density, u_i is the velocity in the i-th direction corresponding to velocity components (u, v, w) and f_k is the mass fraction of species k where $k = 1, 2$ denotes air and hydrogen, respectively. A scalar mixture fraction is used to characterize chemical composition by the non-dimensional density ratio $\phi_1 = (\rho - \rho_2)/(\rho_1 - \rho_2)$, where $\rho_{1,2}$ are the microscopic densities of the air and hydrogen components, respectively and by design $\phi_1 + \phi_2 = 1$. Writing Eq. (3) in terms of ϕ_1 using the relationship $\rho f_1 = \rho_1 \phi_1$ we find:

$$\frac{D\phi_1}{Dt} = \frac{\partial}{\partial x_j}\left(\mathcal{D}\rho \frac{\partial(\phi_1/\rho)}{\partial x_j}\right). \tag{5}$$

The governing equations are discretized following a finite volume formulation with a staggered grid to avoid non-physical checkerboard patterns in the solution [19]. Scalar variables such as pressure and mixture fraction are cell-centered while each velocity component is centered on the face normal to its direction. Staggering also maintains conservation of energy which is important for convergence and to guarantee physically-realizable solutions.

A fractional step method is used to progress the solution through time and allow the use of an explicit advection routine. Velocity and conserved scalar variables are first advected with a Van Leer scheme [20] to avoid spurious oscillations from sharp density and velocity gradients at the interface. After the explicit advection step, intermediate velocities u_i^* are modified with a Lagrangian update of pressure and gravitational source terms from time step n. For example, the starred z-velocities are obtained from the advected velocity $w_t^{n+1/2}$ and source terms:

$$w_t^* = w_t^{n+1/2} + \frac{\Delta t}{\rho_t \Delta z}\left(P_p^n - P_T^n\right) + g_z, \tag{6}$$

Please cite this article in press as: Haley AA, Banerjee A, Role of initial conditions in unstably stratified hydrogen-air mixing zones, International Journal of Hydrogen Energy (2011), doi:10.1016/j.ijhydene.2011.06.001

where starred velocities do not necessarily satisfy Eq. (2). To enforce continuity, velocity corrections, $u_{i,e}{}^{n+1} = u_{i,e}{}^{*} + \Delta u_{i,e}$ and pressure corrections, $p_P{}^{n+1} = p_P{}^{n} + \Delta p_P$ are found from the solution of

$$a_P\Delta p_P + a_E\Delta p_E + a_W\Delta p_W + a_N\Delta p_N + a_S\Delta p_S + a_T\Delta p_T + a_B\Delta p_B = -Div, \quad (7)$$

derived in a manner similar to the SIMPLE [19] approach and solved using a full multi-grid method for enhanced convergence rate. The updated pressure and velocity fields are then used to advect velocity and conserved scalar fields in the next time step. This procedure is repeated for each time step to advance the solution through time.

The scalar transport Eq. (3) includes a Fickian diffusion term which models molecular transport important in gaseous flows. Without this explicit addition, only numerical diffusion would be present, thereby reducing mixing and potentially sacrificing accuracy. The diffusive transport is modeled using a constant mass diffusivity but in the non-Boussinesq form to account for spatial density variation. The domain is treated as periodic in the x and y directions with a slip zero-flux boundary condition enforced at the minimum and maximum z extents.

3. Problem setup

A schematic of the computational domain is shown in Fig. 1. The domain size used in the current study is $L \times L \times 3L$ ($L = 1m$) in x, y, and z, respectively. The initial interface between the two fluids is defined to be in the vertical center of the domain at $z = 1.5L$. Gravity is aligned in the z-direction with a constant magnitude, $g_0 = 9.81\ m/s^2$. A perturbation function is imposed on the interface height, $h_0(x,y)$ from the initial mean interface and then converted to volume fraction through the relation

$$\phi_1(x,y) = \begin{cases} 1 + h_0(x,\ y)/\Delta, & \text{for } h_0 < 0 \\ h_0(x,\ y)/\Delta, & \text{for } h_0 > 0. \end{cases} \quad (8)$$

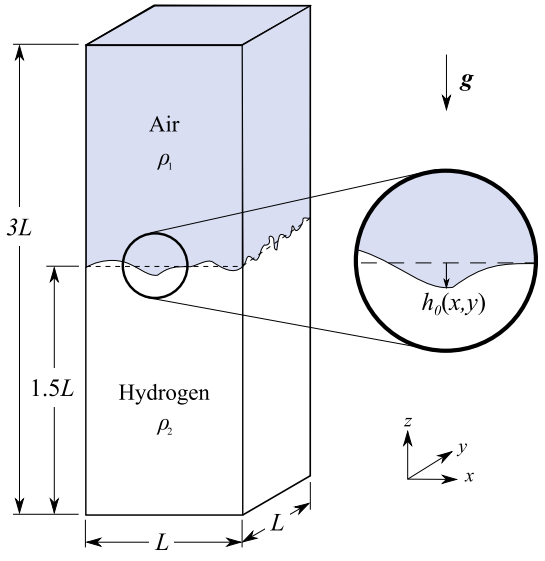

Fig. 1 – Schematic of problem setup (L = 1m).

The simplest permissible interface is the case of an initially flat boundary between the two fluids defined simply by $h_0 = 0$. From linear stability theory we find that this initial condition corresponds to a perturbation amplitude of zero which does not contribute to the instability. Indeed, these initial conditions allow the instability to become sensitive to numerical errors and algorithmic spatial inconsistencies which manifest in perturbation growth from an initially flat (and theoretically quasi-stable) interface [8–10]. As such, these initial conditions should be avoided.

To study the effect of initial conditions on the buoyancy driven flow, multi-mode initial conditions are used having the form

$$h_0(x,y) = \sum_{k_x,k_y} a_k\cos(k_x x)\cos(k_y y) + b_k\cos(k_x x)\sin(k_y y) + c_k\sin(k_x x)\cos(k_y y) + d_k\sin(k_x x)\sin(k_y y), \quad (9)$$

where coefficients a_k, b_k, c_k and d_k are randomly chosen with wave numbers $k = \sqrt{k_x^2 + k_y^2} = 2\pi/\lambda$ selected to give pseudo-random ICs with energy in only the chosen wave number band. Multi-mode initial conditions have a random character and are similar to those observed in experiments. When species diffusion is explicitly modeled we use a constant diffusivity of $\mathcal{D} = 7.6 \times 10^{-5} m^2/s$ consistent with [21] at an assumed temperature of 20 °C.

The ILES technique solves for the Euler's equations and thus no explicit viscous terms are present. However, an effective viscosity is present due to numerical diffusion in the scheme. Thus constraining the problem to $Sc = 1$ (i.e. gases only). Since for hydrogen and air mixtures the Schmidt number is less than unity ($\approx 0.1 - 0.3$) we account for species diffusion explicitly and the technique can be then used as accurate.

4. Results and discussion

Numerical simulations are performed to investigate the effect of ICs, test the Boussinesq (B) approximation for high-Atwood number ($A_t \approx 1$) RT, and evaluate the contribution of an explicitly–modeled species diffusion to mixing. Table 1 lists the cases prepared for the current work. Cases *a-d* are used to investigate the dependence of various mixing parameters on initial perturbation spectra. Cases *e* and *f* complement the

Table 1 – List of simulations.

Run	N_{min}	N_{max}	ρ_1 (kg/m^3)	ρ_2 (kg/m^3)	A_t	g_z/g_0 (m/s^2)	$\mathcal{D}$ (m^2/s)
a	1	32	1.2	0.083	0.87	−1	0
b	4	32	1.2	0.083	0.87	−1	0
c	8	32	1.2	0.083	0.87	−1	0
d	16	32	1.2	0.083	0.87	−1	0
e	4	32	1.2	1.089	0.048	−1	0
f	8	32	1.2	1.089	0.048	−1	0
g	4	32	1.2	0.083	0.87	1	0
h	4	32	1.2	0.083	0.87	1	7.6×10^{-5}
i	1	32	1.2	0.083	0.87	−1	7.6×10^{-5}
j	4	32	1.2	0.083	0.87	−1	7.6×10^{-5}

Please cite this article in press as: Haley AA, Banerjee A, Role of initial conditions in unstably stratified hydrogen-air mixing zones, International Journal of Hydrogen Energy (2011), doi:10.1016/j.ijhydene.2011.06.001

aforementioned runs by allowing examination of comparable configurations with lower density ratios $A_t = 0.048$ and allow isolation and study of non-Boussinesq (NB) effects. Finally, with cases *g–j* the effect of an explicit mass diffusion model in ILES is explored.

Initial conditions are imposed as described in §3. Coefficients a_k, b_k, c_k and d_k in (9) are selected randomly with wave numbers k_x and k_y chosen to give mode number $N_k = Lk/2\pi$ within a specified range (1–32). Initial perturbations for cases *a* and *d* are shown in Fig. 2. The perturbation function $h_0(x,y)$ in the physical domain for runs *a* and *d* shown in Fig. 2a and b demonstrates the initially random character of the perturbations. Fig. 2c and e for run *a* and Fig. 2d and f for run *d* show the discrete range of modes imposed in the initial conditions. Initial perturbation energy is maintained between runs through the relation

$$\frac{\overline{h_0'^2}}{2} = \int_{k_{min}}^{k_{max}} E_{h_0}(k)dk, \tag{10}$$

such that the coefficients in (9) are scaled to give $h_{0,\,rms} = 3.15 \times 10^{-4}$m for all runs.

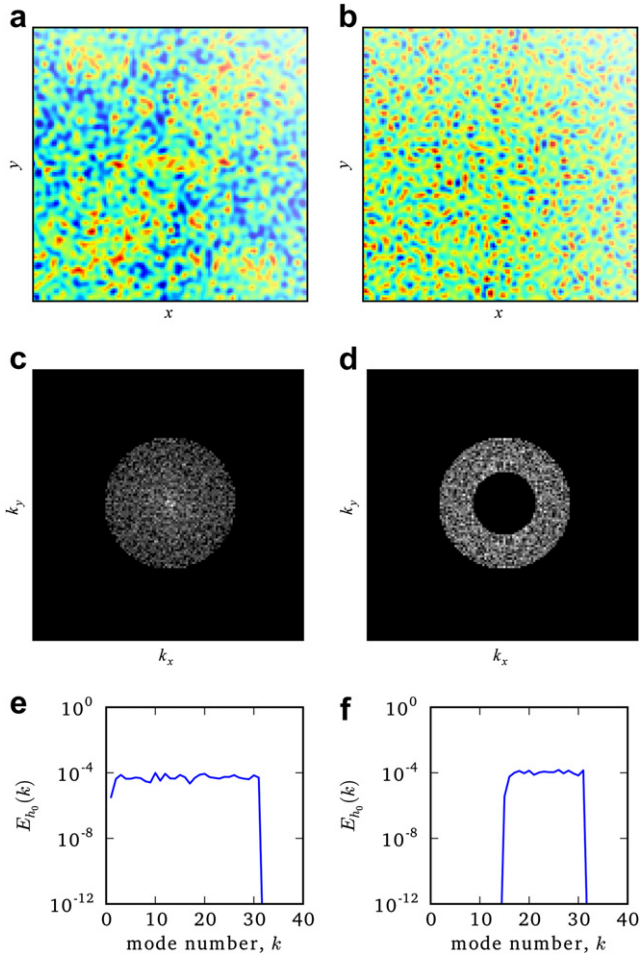

Fig. 2 – Initial perturbation function for runs *a* and *d* in (a), (b) physical and (c),(d) wavenumber space. Azimuthally averaged energy in intial perturbation are also shown in (e) and (f) for runs *a* and *d*, respectively.

The configuration is chosen to be unstably stratified with hydrogen situated below air as in Fig. 1. When perturbed the flow actively seeks a globally lower potential energy through conversion to kinetic energy which in turn drives the flow. Initial perturbations seeded at the interface begin to grow as seen in Fig. 3 leading to progressively more turbulent behavior at later times. As early as $t = 0.4$s, a break in symmetry is seen between the amount of 1–50% (dark) vs. 50–99% (light) hydrogen regions. Also apparent is that the 99% hydrogen front is propagating more effectively, reaching the lower domain extent before the 1% hydrogen front ($t = 2$s). Examination of the isosurfaces of 1% and 99% hydrogen (by volume) as shown in Fig. 4 reveal smooth mushroom-like "bubbles" formed at the 1% hydrogen isosurface and more jagged "spikes" formed at the 99% hydrogen interface. These topological and growth asymmetries arise from the buoyancy effects which drive the flow. Furthermore, the buoyancy forces produce coupling between velocity and density fields that complicates the resulting turbulence leading to a nonlinear dependence on initial conditions.

4.1. *Effect of initial conditions*

In this section the sensitivity of initial perturbations on the mixing process is investigated through quantification of the dependence of various flow parameters on the initial perturbation spectra. Important for comparison with previous work on RT unstable flows, propagation of the mixing front can be tracked through the bubble height h_b defined as the height above the initial interface, z_0 at which the planar averaged mixture fraction

$$\langle \phi_1 \rangle_{z_0} = \iint \phi_1(x, y, z_0)dxdy \tag{11}$$

in plane $z = z_0$ reaches a value of 0.99 (where hydrogen concentration is 1% by volume). Bubble heights for runs *a–d* as displayed in Fig. 5a show little IC dependence at early times with an increasing sensitivity as the flow develops. For direct comparison with previous work we compute the growth rate constant α_b used in the phenomenological equation [22]

$$h_b = \alpha_b A_t g t^2. \tag{12}$$

We use a linear regression for $\sqrt{h_b/L}$ vs. non-dimensional time, $\tau = \sqrt{A_t g t^2/L}$ as suggested by (12) to find α_b, similar to the approach taken by Linden et al [23]. One problem with this technique is that (12) holds only in the late-time regime where the flow has become self similar. For this reason we use h_b to calculate α_b only for $\tau > 2.0$, by which time most of the runs have become self similar. Further, due to the finite domain size, we must be careful to not use h_b beyond a certain time. An upper limit is placed on the computation of growth rates for only $\tau < 4.4$ so that h_b is within 80% of the domain height and thus ensuring the finite domain size has negligible effect [15,24]. An example of the linear fit for run *a* is shown in Fig. 5b. This approach gives a range of α_b from ~ 0.02–0.04 compiled in Table 2. These values are in good agreement with previous work [24].

Of particular interest for development of safety codes is the growth of the lean flammability envelope height over time. To

Please cite this article in press as: Haley AA, Banerjee A, Role of initial conditions in unstably stratified hydrogen-air mixing zones, International Journal of Hydrogen Energy (2011), doi:10.1016/j.ijhydene.2011.06.001

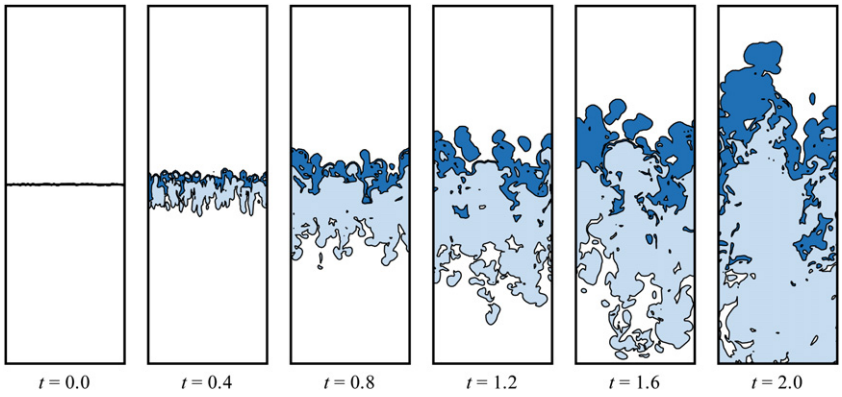

Fig. 3 – Volume fraction isocontours (2D) for run *b*.

study this and the effect of initial conditions, we employ a technique similar to that used to determine h_b but instead define h_l as the height z_0 where $\langle\phi_1\rangle_{z_0} = 0.95$ corresponding to the lower flammability limit of hydrogen in air and thus h_l allows us to track the vertical growth of the flammable zone. Fig. 5c shows a comparison of h_l for runs *a*-*d*. Similar to that seen for h_b, the IC dependence is at first small but grows with time as the non-linear interaction between modes comes into play. Computing α_l in the same way we found α_b gives a range less than that of the latter. Plotting the values of α_b and α_l as a function of $N_{k,min}$ as in Fig. 6 and taking a linear regression fit gives an approximate relationship between α and $N_{k,min}$. We see a negative dependence on $N_{k,min}$ suggesting that lower wave numbers contribute to faster growth. Also, α_b shows a greater sensitivity than α_l to $N_{k,min}$.

From the need to predict explosion hazards, it is important to also track development of the amount of flammable fluid within the simulation domain. Volume of flammable fluid, V_f is defined as the total volume of fluid within the domain that is considered flammable

$$V_f = \iiint \Phi_f(x,y,z)dV. \tag{13}$$

Φ_f is defined as being unity where the fluid has a flammable composition and zero otherwise, eg.

$$\Phi_f = \begin{cases} 0, & \phi_1 < \phi_{LFL} \\ 1, & \phi_{LFL} \le \phi_1 \le \phi_{UFL} \\ 0, & \phi_1 > \phi_{UFL} \end{cases} \tag{14}$$

where $\phi_{LFL} = 0.05$ and $\phi_{UFL} = 0.75$ are the lower and upper flammability limits, respectively. The transient behavior of V_f over time is shown in Fig. 5d for cases *a*–*d*. Good agreement is found for the four cases considered. As V_f is an integral quantity and is therefore less sensitive to individual structures (in contrast to h_b and h_l), it should not be surprising that this parameter shows little sensitivity to ICs.

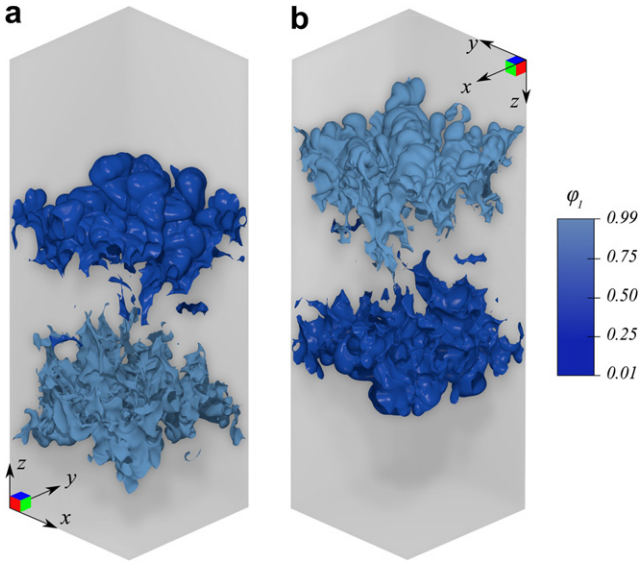

Fig. 4 – Isosurfaces of volume fraction corresponding to 1% (dark) and 99% (light) hydrogen by volume from the perspective of (a) above and (b) below the initial interface plane.

4.2. *Non-boussinesq effects*

The B approximation, used primarily to simplify analysis and simulation, essentially replaces the acceleration term g with a reduced gravity $g' = g\Delta\rho/\bar{\rho}$ where $\bar{\rho} = 1/2(\rho_1 + \rho_2) \approx \rho$ for $\Delta\rho = (\rho - \bar{\rho}) << \bar{\rho}$. Thus the B approximation holds only for low density ratios, or, equivalently, for $A_t << 1/2$. In the current study we wish to qualitatively study and then quantify the NB effects.

First we examine qualitative nature of the difference between a B case, run *e* ($A_t = 0.048$), with the NB case, run *b* ($A_t = 0.87$). Fig. 7 shows slices from the B case run *e*. Unlike the NB case shown in Fig. 3, a symmetry is observed between the structures formed at 1% and 99% fluid boundaries. The general structure growth appears qualitatively similar otherwise (albeit at a slower rate). Bubble and spike heights, h_b and h_s respectively, are plotted against non-dimensional time, τ in Fig. 8. Good agreement is seen between runs for h_b, but h_s is larger for the NB case. This is expected as typically spikes tend toward the free-fall limit of $\alpha_s \to 0.5$ as $A_t \to 1$, but are found to converge to α_b in the limit $A_t << 1$ [23,25]. Thus we find that the spikes are grossly under-predicted if the B approximation is applied in the present study. Computing α_b for runs *e* and *f* (see Table 2) and comparing with runs with the same initial

Please cite this article in press as: Haley AA, Banerjee A, Role of initial conditions in unstably stratified hydrogen-air mixing zones, International Journal of Hydrogen Energy (2011), doi:10.1016/j.ijhydene.2011.06.001

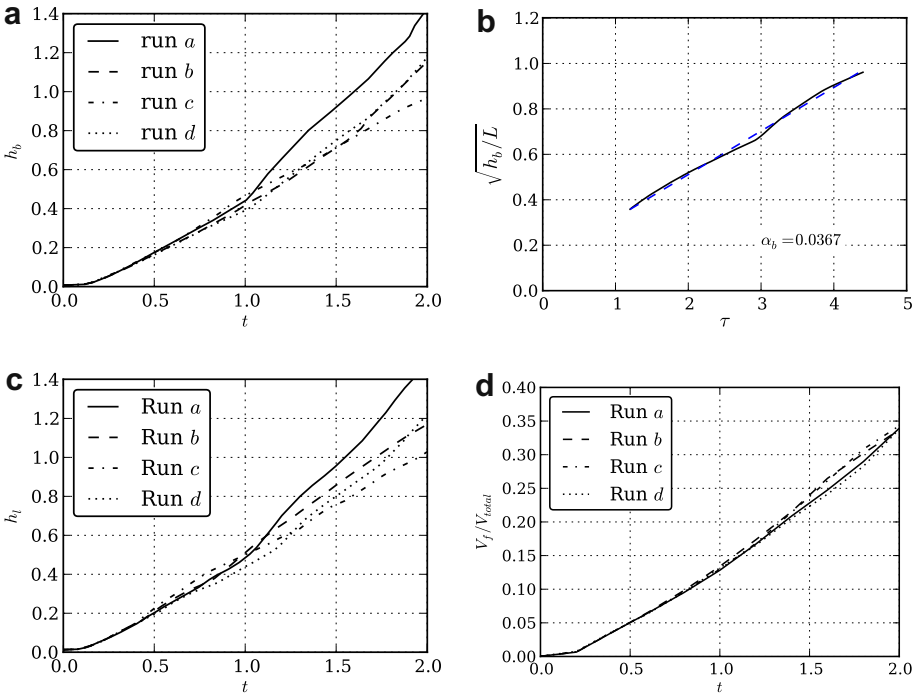

Fig. 5 – Plots of (a) h_b, (c) h_l, and (d) V_f over time for various initial perturbation spectra with (b) example linear regression fit for growth rate.

Table 2 – Computed growth rates.

Run	α_b	α_l
a	0.0367	0.0239
b	0.0224	0.0233
c	0.0214	0.0261
d	0.0248	0.0210
e	0.0233	–
f	0.0180	–
i	0.0317	0.0206
j	0.0181	0.0166

condition spectra, runs *b* and *c* respectively, shows that α_b is much more robust to deviations from the B limit than α_s.

Now we turn our attention to profiles of planar-averaged air mixture fraction $\langle\phi_1\rangle$ in Fig. 9. At similar times ($\tau \approx 3$) the NB case, run *b*, develops asymmetry with respect to the initial interface in the left and right tail. The left tail represents the lower portion of the domain with hydrogen-rich mixture whereas the right tail the upper, fuel-lean zone. The right tail shows decent agreement with respect to the B and NB cases with a similar shape and maximum. The left tail however showcases the deviation in the NB case as it approaches $\langle\phi_1\rangle = 0$ at a much lower location $z/L \approx 0.5$ compared to $z/L \approx 1$ for the B case. Density variation enters into the B governing equations only through the reduced gravity term g' and thereby forcing the flow be symmetric (or invertible). Thus only the NB formulation can correctly reproduce the non-symmetric mixture fraction profile.

Furthermore in the NB case, density fluctuations have minimal impact on overall mixing dynamics. For example, a density fluctuation of 10% in either species would represent only about a 1% change in A_t (because the Atwood number is large in the NB case). Conversely in the Boussinesq limit, fluctuations in species density gives rise to much larger

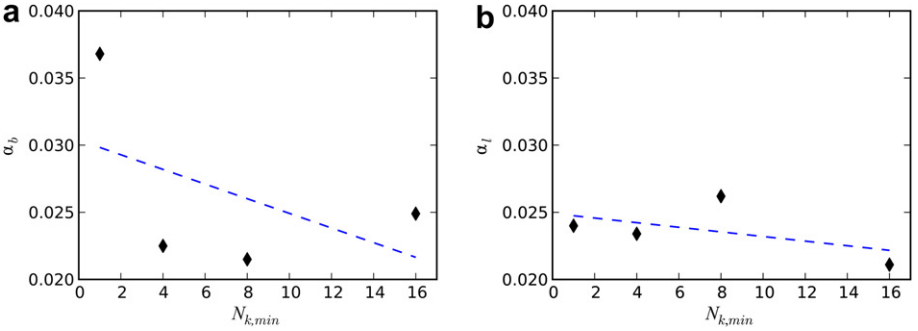

Fig. 6 – Linear fit of (a) α_b and (b) α_l versus $N_{k,min}$.

Please cite this article in press as: Haley AA, Banerjee A, Role of initial conditions in unstably stratified hydrogen-air mixing zones, International Journal of Hydrogen Energy (2011), doi:10.1016/j.ijhydene.2011.06.001

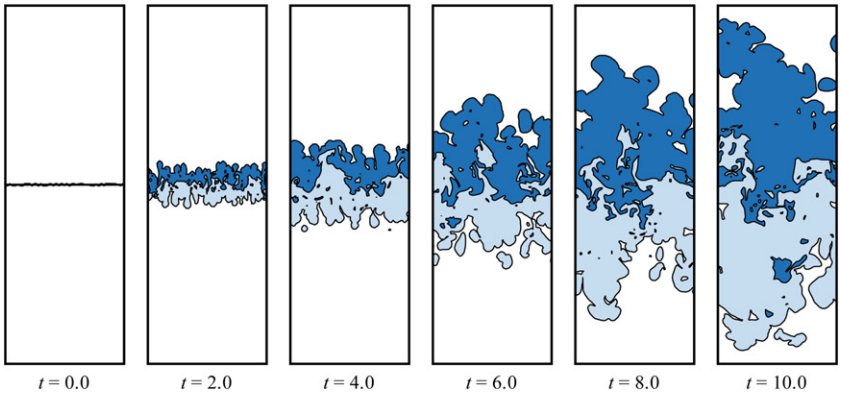

Fig. 7 – Isocontours of volume fraction across a slice for the Boussinesq run *e*.

variation in A_t. Robustness to global density fluctuations is another unique feature of NB flows.

4.3. *Explicit species diffusion*

Molecular mixing is an important part of the overall mixing process and as such requires special attention when modeling. Here we investigate the effect of using an explicit diffusion model (as opposed to the numerically-implied scheme used until now). To account for molecular mixing we use a species diffusivity $\mathcal{D} = 7.6 \times 10^{-5}$ m/s^2 and Fickian flux modeled by the last term in Eqn. (3).

In the stable case of hydrogen situated above air of Fig. 10, there is no instability and the initial perturbations at the interface do not grow. In the case where no explicit diffusion is accounted for the interface remains sharp, Fig. 10a. For the diffusive case of Fig. 10b mixing occurs due to the explicit diffusion model. As the initially sharp interface becomes blurred, the driving gradient is diminished and thus rate of dispersion decreases. Asymmetry is observed when showing the profile of planar averaged ϕ_1 variation in the vertical direction as in Fig. 10c. The asymmetry is attributed to the NB model used for species flux.

Transient development of run *j* is shown in Fig. 11 where explicit diffusion modeling is used. Compared to run *b*, Fig. 3, it appears that the added diffusion tends to smear out smaller structures. Plotting h_b for two diffusive cases, runs *i* and *j*, and two non-diffusive cases, runs *a* and *b*, in Fig. 12a we see that the effect of the added diffusive flux tends to reduce the growth of the hydrogen dispersion envelope somewhat. As a consequence α_b is reduced by ~16%. Similarly, plotting flammability envelope height h_l for the four aforementioned runs shows that the explicit species diffusion model contributes to little variation in height magnitude, however growth rate constant α_l decreased by ~ 20%, comparable to the decrease in bubble growth rate constant. Plotting V_f for runs *a*, *b*, *i*, and *j* in Fig. 12c shows that flammability volume is relatively insensitive to both ICs and species diffusion model (implicit or explicit in this case). The small change in overall mixing can be explained as the two main forces driving mixing, dispersion by buoyancy-driven turbulence and molecular diffusion, are counteracted when using an explicit model for species diffusivity. As diffusion increases, the dispersion of hydrogen tends to decrease because the smoothing effect the instability. However, the lower dispersion is offset by increased mixing from increased species diffusivity.

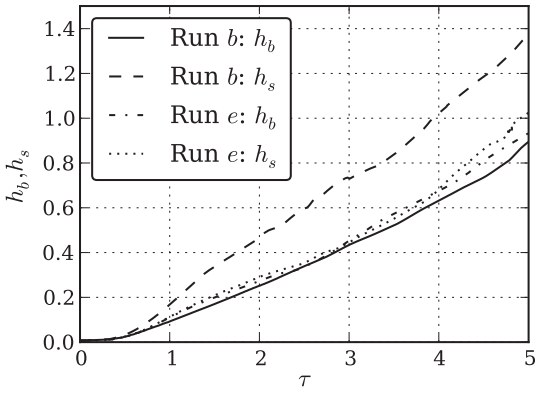

Fig. 8 – Bubble and spike heights for runs *b* and *e* depicting the spike growth divergence for high A_t RT (run *b*).

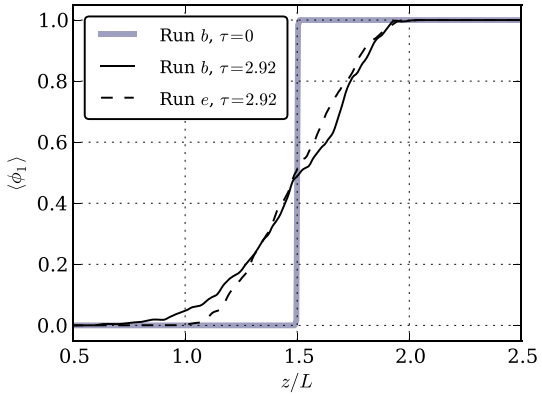

Fig. 9 – Profiles of planar averaged mixture fraction for NB (run *b*) and B (run *e*) cases highlighting break in symmetry for NB case. Initial profile is also shown as thick shaded line for reference.

Please cite this article in press as: Haley AA, Banerjee A, Role of initial conditions in unstably stratified hydrogen-air mixing zones, International Journal of Hydrogen Energy (2011), doi:10.1016/j.ijhydene.2011.06.001

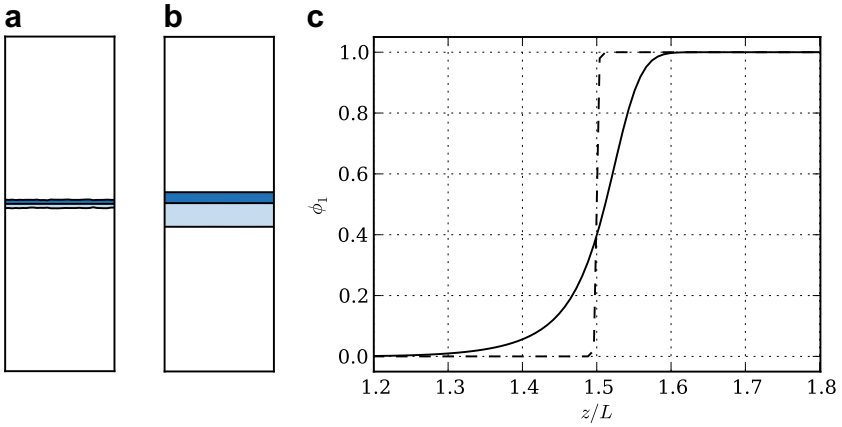

Fig. 10 – Comparison of isocontours for stable cases using (a) an implicit and (b) Fickian diffusion models at t = 100s. Volume fraction profiles shown in (c) for explicit (solid line) and numerically implied (dashed line) models.

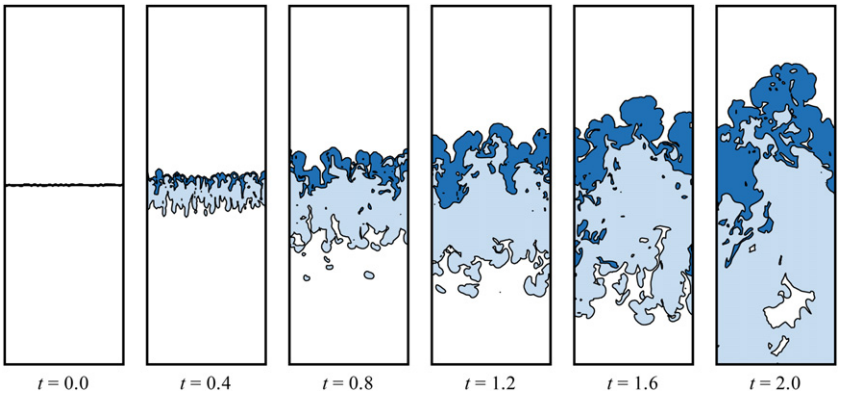

Fig. 11 – Volume fraction isocontours unstably stratified hydrogen and air from run *j* (Fickian model of species diffusivity).

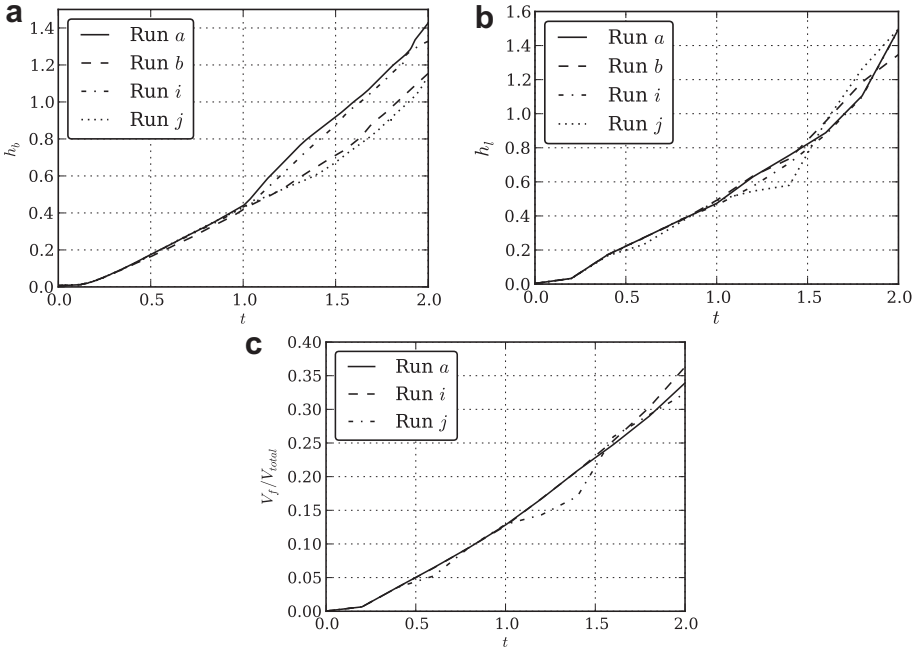

Fig. 12 – Comparison of (a) h_b (b) h_l, and (c) V_f for implicit and explicit species diffusion models.

Please cite this article in press as: Haley AA, Banerjee A, Role of initial conditions in unstably stratified hydrogen-air mixing zones, International Journal of Hydrogen Energy (2011), doi:10.1016/j.ijhydene.2011.06.001

5. Conclusions

Hydrogen-air mixing was investigated through use of an implicit large eddy simulation code to study the effect of initial conditions as well as non-Boussinesq effects and the contribution of an explicit diffusivity model to mixing. Initial conditions were precisely controlled and characterized to determine the effect of smallest mode numbers on mixing. Sensitivity to ICs was shown to become more important as time progressed through tracking the propagation and growth of flammability zones. It was shown that lean flammability envelope height, h_l, varies as much as 14% and has a negative dependence on the smallest imposed mode, $N_{k,min}$. Likewise a much larger drop in growth rate for bubble height, h_b, was seen of around 40% with a stronger dependence on $N_{k,min}$. Fraction of flammable fluid, V_f, however was shown to be much less sensitive to initial perturbation. It was also shown that air-hydrogen mixing is inherently non-Boussinesq and cannot be modeled as a Boussinesq flow. Characteristics of a non-Boussinesq flow such as mixing-zone growth asymmetries cannot be replicated. An explicit species diffusion model was compared with results using the one implied from the numerical scheme. We find that little effect is shown for V_f but that growth rates, α_b and α_l are reduced significantly.

The initial perturbation spectrum is highly dependent upon the accidental release scenario. The present work examines a range of initial perturbations to examine and quantify the effect of the initial state on mixing without regard to a specific release situation. Numerical computations naturally are greatly aided by using a representative initial state when simulating an accidental release. However in this case we examine a wide range of perturbations within the resolvable scales to study the overall effect–a case by case perturbation analysis is left for future efforts.

Acknowledgments

The authors acknowledge the CBET-Fluid Dynamics program at the U.S. National Science Foundation (Award Number 0967672) for providing funding for this research. The authors would also like to thank Dr. Malcolm J. Andrews for permitting use of his code RTI-3D.

REFERENCES

[1] Koroneos C, Dompros A, Roumbas G, Moussiopoulos N. Life cycle assessment of hydrogen fuel production processes. Int J Hydrogen Energy 2004;29:1443–50.
[2] U.S. Department of Energy. Hydrogen Posture Plan: an Integrated Research, development and Demonstration Plan. U.S. Department of Energy; 2006.
[3] Heitsch M, Baraldi D, Moretto P. Numerical analysis of accidental hydrogen release in a laboratory. Int J Hydrogen Energy 2010;35:4409–19.
[4] El-Amin MF. Non-Boussinesq turbulent buoyant jet resulting from hydrogen leakage in air. Int J Hydrogen Energy 2009;34:7873–82.
[5] Swain M, Filoso P, Swain M. An experimental investigation into the ignition of leaking hydrogen. Int J Hydrogen Energy 2007;32:287–95.
[6] Houf W, Schefer R. Analytical and experimental investigation of small-scale unintended releases of hydrogen. Int J Hydrogen Energy 2008;33:1435–44.
[7] Cariteau B, Brinster J, Tkatshenko I. Experiments on the distribution of concentration due to buoyant gas low flow rate release in an enclosure. Int J Hydrogen Energy 2011;36:2505–12.
[8] Cisse P, Karim GA. The rapid formation and dispersion of flammable zones within cylindrical vertical enclosures following the release of a fixed mass of hydrogen and other gaseous fuels into air. Int J Hydrogen Energy 2007;32:630–6.
[9] Fardisi S, Karim GA. Characteristics of flammable, buoyant hydrogen plumes rising from open vertical containers. Int J Hydrogen Energy 2009;34:6568–79.
[10] Vudumu SK, Koylu UO. Detailed simulations of the transient hydrogen mixing, leakage and flammability in air in simple geometries. Int J Hydrogen Energy 2009;34:2824–33.
[11] Wilkening H, Baraldi D. CFD modelling of accidental hydrogen release from pipelines. Int J Hydrogen Energy 2007;32:2206–15.
[12] Prasad K, Pitts WM, Yang JC. A numerical study of the release and dispersion of a buoyant gas in partially confined spaces. Int J Hydrogen Energy 2011;36:5200–10.
[13] Rayleigh Lord. Scientific Papers, vol. II. Cambridge, England: Cambridge University Press; 1900.
[14] Taylor GI. The instability of Liquid Surfaces when Accelerated in a direction Perpendicular to their Planes. I. Proc Royal Soc London Ser A Math Phys Sci 1950;201(1065):192–6.
[15] Banerjee A, Andrews M. 3D Simulations to investigate initial condition effects on the growth of Rayleigh–Taylor mixing. Int J Heat Mass Transfer 2009;1:3906–17.
[16] Cabot A, Dimotakis P. Transition stages of Rayleigh–Taylor instability between miscible fluids. J Fluid Mech 2001;443:69–99.
[17] Chandrasekhar S. Hydrodynamic and Hydromagnetic stability. New York: Dover Publications, ISBN 048664071X; 1981.
[18] Andrews MJ. Accurate computation of convective transport in transient two-phase flow. Int J Numer Methods Fluids 1995;21:205–22.
[19] Patankar S. Numerical Heat Transfer and fluid flow. Washington: Hemisphere Pub. Corp, ISBN 0891165223; 1980.
[20] Leer BV. Towards the ultimate conservative difference scheme. IV. A new approach to numerical convection. J Comp Phys 1977;23(3):276–99.
[21] Marrero TR, Mason EA. The diffusion of atoms and molecules. J Phys Chem Ref Data 1972;1:3–118.
[22] Read KI. Experimental investigation of turbulent mixing by Rayleigh-Taylor instability. Physica D 1984;12:45–58.
[23] Linden PF, Redondo JM, Youngs DL. Molecular mixing in Rayleigh-Taylor instability. J Fluid Mech 1994;265:97–124.
[24] Dimonte G, Youngs DL, Dimits A, Weber S, Marinak M, Wunsch S, et al. A comparative study of the turbulent Rayleigh–Taylor instability using high-resolution three-dimensional numerical simulations: the Alpha-Group collaboration. Phys Fluids 2004;16(5):1668–93.
[25] Ramaprabhu P, Dimonte G. Single-mode dynamics of the Rayleigh-Taylor instability at any density ratio. Phys Rev E; 2005:71.

Please cite this article in press as: Haley AA, Banerjee A, Role of initial conditions in unstably stratified hydrogen-air mixing zones, International Journal of Hydrogen Energy (2011), doi:10.1016/j.ijhydene.2011.06.001